Sensors and Materials, Vol. 26, No. 4 (2014) 235–244
MYU Tokyo

S & M 0987

Analysis of Temperature Dependence of Dark Current Mechanisms in Mid-Wavelength Infrared pin Type-II Superlattice Photodiodes

Jarosław Wróbel*, Elena Plis[1], Waldemar Gawron, Marcin Motyka[2], Piotr Martyniuk, Paweł Madejczyk, Andrzej Kowalewski, Mateusz Dyksik[2], Jan Misiewicz[2], Sanjay Krishna[1] and Antoni Rogalski

Institute of Applied Physics, Military University of Technology,
2 Kaliskiego St., 00-908 Warsaw, Poland
[1]Department of Electrical and Computer Engineering, Center for High Technology Materials,
University of New Mexico, Albuquerque, New Mexico 87106, USA
[2]Institute of Physics, Wroclaw University of Technology,
Wybrzeże Wyspiańskiego 27, 50-370 Wrocław, Poland

(Received November 21, 2013; accepted February 24, 2014)

Key words: dark current, type II, superlattice, photodiode, differential resistance, infrared detection, high operating temperature, reduced mass, pin structure

We report on the temperature dependence characteristics of mid-wavelength InAs/GaSb type-II superlattice photodiodes in a temperature range from 120 to 240 K. The bulk material model with an effective bandgap of superlattice material has been used in the modelling of the experimental data. Temperature and bias-dependent differential resistances have been analyzed in detail owing to the contributing mechanisms that limit the electrical performance of the diodes. The C1-HH1 reduced mass has been estimated from the fitting to the high reverse bias (< –1.0 V) voltage and given as about 0.015 m_0 in nearly the entire considered temperature range. This value agrees well with much more complex simulations and cyclotron resonance measurements. Obtaining very good results was possible, thanks to the inclusion of series resistance into the calculations. In this paper, we show how to overcome difficulties with the nonlinear problem related to it.

1. Introduction

In the middle of the 1970s, investigations on the InAs/GaSb superlattice (SL) near lattice-matched systems were performed as an alternative to the GaAs/AlAs SLs. The ability of the InAs/GaSb material system to achieve small infrared (IR) energy gaps was first realized in 1977.(1) At once, the type II band offset in this system was revealed(2) and the potential use of this system in IR photoelectronics was recognized. At present,

*Corresponding author: e-mail: jarekwrobel@wat.edu.pl

the InAs/GaSb strained layer SLs (SLSs) are considered as alternatives to HgCdTe IR material systems[3] and a candidate for third-generation IR detectors[4] as well as in high operating temperature (HOT).[5]

In this paper, we focused on one of the possible constructions of the mid-wavelength IR (MWIR) InAs/GaSb SL photodiodes, namely, pin structures. We concentrate here on a dark current modelling to point out which components limit the device performance at a determined bias voltage and temperature regime. Because counting nonequilibrium states and current flow direct from the SL band structure (even for the ideal crystal approximation) is rather complicated (see *e.g.* ref. 6), bulklike modelling is often used.[7–11] In most cases, researchers have focused on a cryogenic application and region close to the zero bias voltage, where the series resistance (R_{series}) is usually neglected, owing to its small value (compared with R_{device}). In this paper, we extend analyses up to the HOT conditions, from 120 to 240 K, and bias voltage from –1.6 to +0.3 V. We show how to overcome the difficulties related to taking into account R_{series}, in the simplest situation, i.e., with no exclusion effect. Finally, we compare some of the fitting results, i.e., m^*_{red} for C1-HH1 transition [see eq. (7)], with available literature data.

2. Growth and Device Design

The representative sample presented in this work is the InAs/GaSb SLS pin detector with the SU-8 passivation fabricated at the Center for High Technology Materials, University of New Mexico, Albuquerque, New Mexico. The device structure was grown on Te-doped epiready (100) GaSb substrates. It consists of 100 periods of ten monolayers (10 MLs) of InAs:Si ($n = 4 \times 10^{18}$ cm^{-3})/10 MLs of GaSb as the bottom contact layer. This was followed by 50 periods of graded n-doped 10 MLs of InAs:Si/10 MLs of GaSb, 350 periods of absorber, 25 periods of 10 MLs of InAs:Be ($p = 1 \times 10^{18}$ cm^{-3})/10 MLs of GaSb, and finally, 17 periods of 10 MLs of InAs:Be ($p = 4 \times 10^{18}$ cm^{-3})/10 MLs of GaSb, which formed a p-type contact layer.

A normal-incidence single-pixel mesa photodiode, with a 450 × 450 μm^2 electrical area, was fabricated by photolithography and inductively coupled plasma etching. Ohmic contacts were made by depositing Ti/Pt/Au on the contact layers. For details, see ref. 12.

3. Experimental Results

For the experiments, we have chosen two samples with the same design (see Fig. 1) and electric areas, but essentially different R_{shunt} and R_{series}. This approach could give us information that the presented model is independent of these resistance values (see discussion in §§ 4 and 5). The dark current-voltage characteristics were measured in the temperature range of 120–240 K using a Keithley 2400 Source Meter (see Fig. 2). The differential resistances at different temperatures were calculated on the basis of the dark current data and presented in Fig. 3. The explanation of the shapes of these characteristics and the description of the mechanisms that govern current flow are provided by theoretical modelling (see § 4).

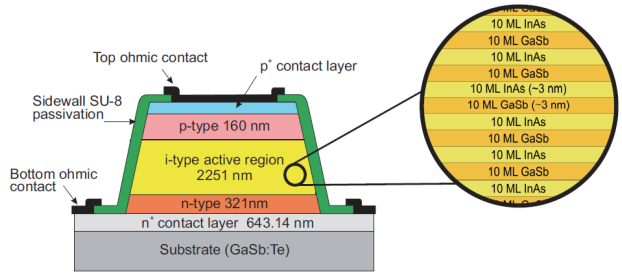

Fig. 1. (Color online) Single-pixel InAs/GaSb superlattice pin photodiode (not to scale).

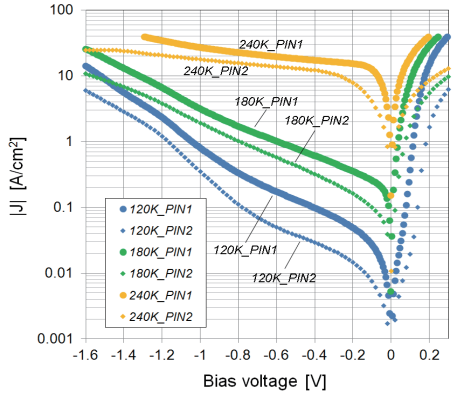

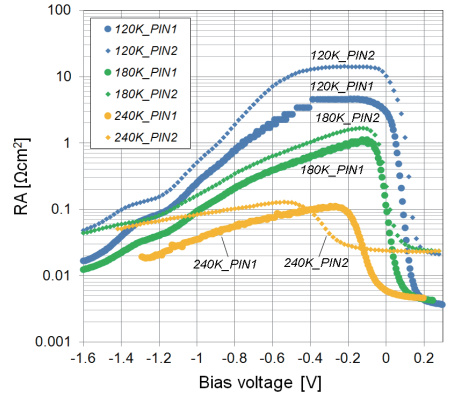

Fig. 2 (left). (Color online) Dark current density-voltage characteristics of type-II SL photodiodes at different temperatures.
Fig. 3 (right). (Color online) Differential resistance-area products versus bias voltage of type-II SL photodiodes at different temperatures.

Next, the Fourier-transformed IR (FTIR) photoluminescence (PL) spectra were measured to obtain the variation of the effective bandgap (E_g) of our structure with temperature and to confirm the existence of the inter-bandgap states, which we have taken into account in the dark current modelling. To measure FTIR PL spectra, we used a Bruker spectrometer Vertex 80v in a step-scan mode together with an external chamber for experiments with an additional modulated beam (the scheme of the setup and more details can be found in ref. 13). This configuration allows us to make all the measurements with the complete optical path totally under vacuum (1.5×10^2 Pa), which is an important advantage in the case of making measurements in the mid- and far-IR regions where a number of atmospheric gas absorption bands can disturb the detected signal intensity. In these measurements, a liquid-nitrogen-cooled MCT photodetector was used. The pump beam was provided by the 660 nm line of a semiconductor laser diode and then mechanically chopped at a frequency of 275 Hz. A phase-sensitive detection of the optical response was performed using a lock-in amplifier.

In Fig. 4, the FTIR PL spectrum obtained (at 20 K) for the PIN InAs(10 ML)/GaSb(10 ML) sample without any electrical contacts is shown. In this graph, three features can be easily recognized. First, the peak at the energy higher than 700 meV should be connected to recombine in the forbidden gap of the doped GaSb layer. Second, that observed at ~225 meV has been recognized as a fundamental PL between the first electron and the first heavy hole levels in InAs/GaSb SLs. The weakest signal measured for the energies lower than 100 meV was associated with carrier recombination thru the defect states located in the energy gap of the investigated SL. Qualitatively similar results have been observed before in the electroluminescence (EL) spectra for the long-wavelength IR (LWIR) devices.[14] The inset of this graph shows the temperature dependence of the fundamental transition in the SL. Owing to the doped GaSb cap layers, the PL signal was obtained only for low temperatures (up to 80 K). Nevertheless, these values seem to be in good agreement with the energies presented by Klein *et al*. (which were obtained from $\lambda_{50\%\text{cutoff}}$ of the absorption spectrum data).[12]

Thus, the variation of the effective bandgap (E_g) with temperature (T), which was used in our calculation, is the same as that given by Klein *et al.*

$$E_g = 0.234 - 3.1 \cdot 10^{-4} \cdot \frac{T^2}{T + 270} \quad [\text{eV}] \tag{1}$$

The intergap state emission and the interesting small blue shift of the main peak with temperature will be the subjects of a different contribution.

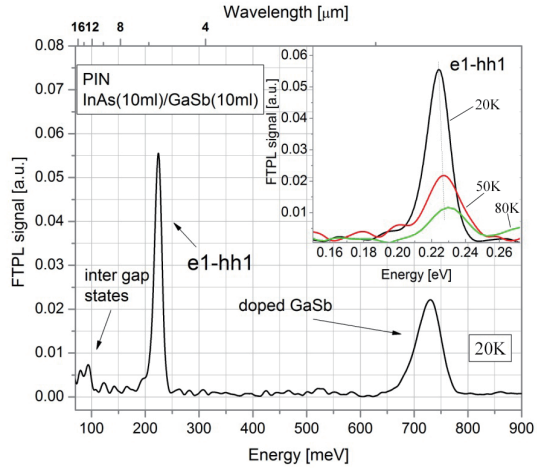

Fig. 4. (Color online) FTIR PL spectra of $InAs_{10ML}/GaSb_{10ML}$ SL sample.

4. Modelling of Current-Voltage Characteristics

To explain the current-voltage characteristics of the MWIR type-II SLS pin photodiodes, a bulk material model with an effective bandgap of the SL material is used. We assumed here that only two minibands essentially affect the electronic properties of the diode, namely, C1 and HH1. Additionally, we have taken into account the band anisotropy and adapted it to the commonly used Shockley relations for the single pn junction[7–11] (the second junction is isotype and is usually neglected, because of its negligibly small resistance in this case).

In general, our model is based on the standard assumption that the photodiode dark current density can be found as a superposition of several mechanisms (see Fig. 5):

$$J_{\text{dark}} = J_{\text{diff}} + J_{\text{gr}} + J_{\text{btb}} + J_{\text{tat}} + J_{R\text{shunt}}, \tag{2}$$

i.e., diffusion (J_{diff}), generation-recombination (J_{gr}), band-to-band tunnelling (J_{btb}), and trap-assisted tunnelling (J_{tat}). The remaining mechanisms are current owing to the shunt resistance ($J_{R\text{shunt}}$ originates from the surface and bulk leakage current) and R_{series}. The first fundamental component, J_{diff}, where we assumed the reflective contact configuration,[15,16] is given by

$$J_{\text{diff}} = qn_i^2 \left(\frac{D_{\text{e}}}{N_{\text{a}} L_{\text{e}}} \tanh \frac{x_{\text{p}}}{L_{\text{e}}} + \frac{D_{\text{h}}}{N_{\text{d}} L_{\text{h}}} \tanh \frac{x_{\text{n}}}{L_{\text{h}}} \right) \times \left[\exp\left(\frac{qV}{kT} - 1 \right) \right], \tag{3}$$

where q is the electron charge, k is Boltzmann's constant, T is the absolute temperature, $L_{\text{e,h}}$ is the electron/hole diffusion length, $D_{\text{e,h}}$ is the diffusivity ($L_{\text{e,h}}$ and $D_{\text{e,h}}$ are connected with the diffusion lifetime $\tau_{\text{e,h}}$ and mobilities $\mu_{\text{e,h}}$ by Einstein relations), $N_{\text{a,d}}$ denotes acceptor/donor doping concentrations, and $x_{\text{n,p}}$ are the thicknesses of the n,p-type regions. The intrinsic carrier concentration n_i can be approximated by

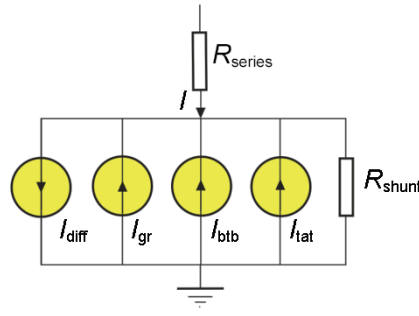

Fig. 5. (Color online) Equivalent circuit diagram.

$$n_i^2 = N_c N_v \exp\left(-\frac{E_g}{kT}\right), \tag{4}$$

where the density of states of electron/holes ($N_{c,v}$) is defined as

$$N_{c,v} = 2\left(\frac{kTm^*_{e,h\ DOS}}{2\pi\hbar}\right)^{3/2}, \tag{5}$$

and the density of states of effective masses ($m^*_{e,h\ DOS}$) is defined as

$$m^*_{e,h\ DOS} = (m^{*2}_{c1,hh1//}\, m^*_{c1,hh1\perp})^{1/3}, \tag{6}$$

whereas the reduced mass (m^*_{red}) in the C1-HH1 transition is taken as

$$m^{*\,-1}_{red} = m^{*\,-1}_{c1//} + m^{*\,-1}_{hh1//}, \tag{7}$$

because of the nonnegligible oscillator strength only in the in-plane direction.[17]

This causes the C1-HH1 band-to-band tunneling to take the form of

$$J_{btb} = \frac{\sqrt{2m^*_{red}q^3EV}}{4\pi^2E\hbar\sqrt{E_g}}\exp\left(-\frac{4\sqrt{2m^*_{red}}E_g^{3/2}}{3qE\hbar}\right), \tag{8}$$

where, for an abrupt pn junction, the electric field E can be approximated as[4]

$$E = \left[\frac{2q}{\varepsilon_0\varepsilon_s}\left(\frac{E_g}{q} - V\right)\frac{N_aN_d}{N_a + N_d}\right]^{1/2}. \tag{9}$$

Under a strong built-in field, the chance that an electron-hole pair becomes separated and collected at the electrode is much higher than that for a pair outside the depletion layer. The generation-recombination current, J_{gr}, is a major current source in diodes with a high density of defects in the depletion region. We can approximate it as

$$J_{gr} = \frac{qn_iw}{\tau_{gr}}\frac{2\sinh\left(\frac{qV}{2kT}\right)}{\frac{q(V_b - V)}{kT}}f(b), \tag{10}$$

where $f(b)$ is a complicated expression involving a trap level and an applied voltage,[9] and w is the depletion width that depends on the applied bias V and the built-in potential V_b as[4]

$$w = \sqrt{\frac{2\varepsilon_0\varepsilon_r}{q}\frac{N_d + N_a}{N_a N_d}(V_b - V)}. \quad (11)$$

The second mechanism bounded with states inside the bandgap is the trap-assisted tunnelling. Similarly to our previous paper,[18] we assumed that it is responsible for the tunnelling-like behaviour in the bias voltage from about –0.4 to –0.6 V. The simplified formalism, introduced by Kinch[19] and Yang *et al.*,[20] has shown that

$$J_{tat} = \frac{q^2 m_t^* M^2 N_t V}{8\pi\hbar^3(E_g - E_t)}\exp\left[-\frac{4\sqrt{2m_t^*}(E_g - E_t)^{3/2}}{3qE\hbar}\right], \quad (12)$$

where N_t is the activated trap density, m^*_t is the effective tunnelling mass (generally different from m^*_{red}), E_t is the effective trap energy level, measured from the valence band edge, and M^2 is the matrix element associated with the trap potential, assumed to be 10^{23} eV^2cm^3.

Additionally, we took into consideration the shunt resistance, which is clearly seen in the low-temperature regime (see Fig. 3). In this case, we assumed bias voltage independence. A similar assumption was made for the R_{series}, but taking it into account is more difficult because of the connection of this mechanism to all the rest (see Fig. 5). To avoid difficulties in solving a nonlinear problem at every *I-V* point, one can use the following simple technique:

1. calculate all components of dark current without series resistance (V in the relations above means applied voltage on the ideal structure, i.e., without series resistance)
2. calculate the voltage drop on a series resistance using the current value estimated in the previous point, from the simple Ohm's law (R_{series} can be estimated from the forward bias voltage region of a differential resistance-voltage characteristic for each temperature), and
3. add voltages used in the 1st and calculated in the 2nd point. This gives us the voltage drop that is connected to the previously calculated J_{dark}, which can be compared now with the experimental *I-V* point.

As one can see, the voltage drop on the entire structure is calculated, not assumed to be given as an input parameter. We should underline here that this technique is correct only for the situation, where no exclusion effect is observed —i.e., where increasing $|V|$ always causes increasing $|J_{dark}|$. It is also worthy mentioning here that assuming $R_{series} = 0$ might cause serious over- or underestimation of some fitting parameters under the HOT regime.[21] One of the clearly visible effects connected to this problem is related to the deformation of R_{shunt}. This plot should be symmetric if R_{series} would be much lower than R_{device}. Because it is not true for all bias voltage points, all components of J_{dark} are tensioned (effectively shifted to higher values of $|V|$), especially in the forward bias part of the *I-V*s. The values of the parameters used in a device modelling are the same as those in ref. 18.

5. Results and Discussion

The model briefly described in our previous paper[18] and more detailed in § 4 assumes that there are eight not well-known parameters: m^*_{red}, m^*_t, E_t, N_t, τ_{diff}, τ_{gr}, R_{shunt}, and R_{series}. Each of them can be obtained through a fitting to the experimental data. For example, R_{series} should limit the dark current in the linear part of a forward bias voltage [see Figs. 6(b) and 7(b), at V = 0.3 V] in a device with a single junction dominance. Similarly, we predict that the tunneling-like behaviour in a high reverse bias voltage [see Figs. 6(b) and 7(b) for a region from about –0.9 to –1.6 V] should be related to the transition between the closest minibands with the highest population of levels (in our

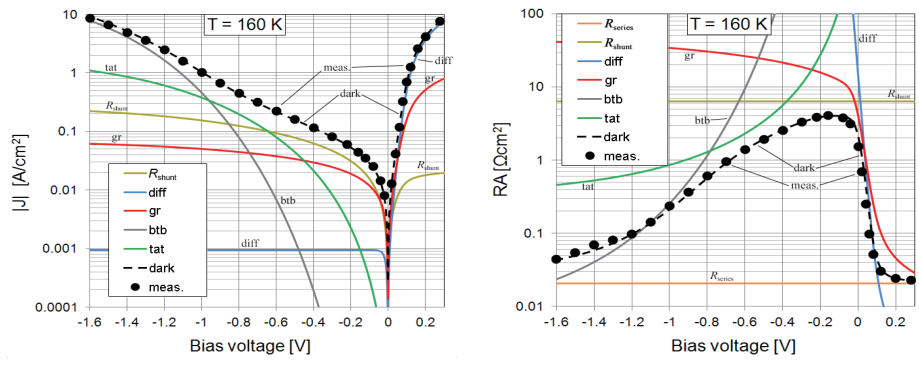

(a) (b)

Fig. 6. (Color online) Example of measured and modelled characteristics of the PIN_2 MWIR $InAs_{10ML}/GaSb_{10ML}$ type-II SL photodiode at 160 K: dark current density (a) and resistance-area product (b) vs bias voltage.

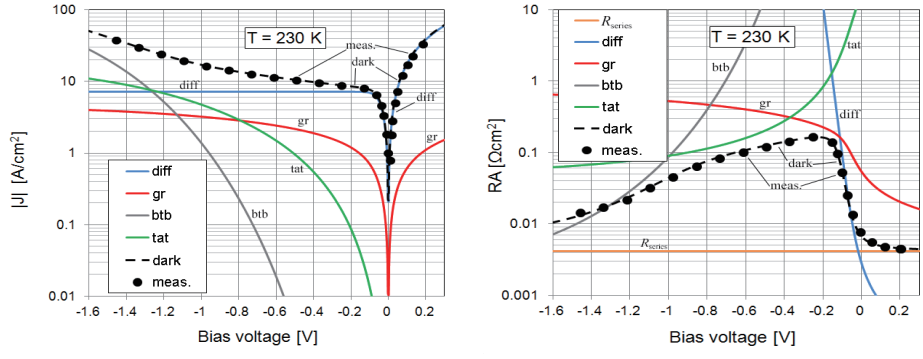

(a) (b)

Fig. 7. (Color online) Example of measured and modelled characteristics of the PIN_1 MWIR $InAs_{10ML}/GaSb_{10ML}$ type-II SL photodiode at 230 K: dark current density (a) and resistance-area product (b) vs bias voltage.

case, C1 and HH1). Because the single, not well-known parameter in eq. (8) is m^*_{red} and the band-to-band mechanism dominates in this bias region, we can treat the fitting result of this parameter as a "measured" value. However, this point of view should be taken as a rough estimation, at least, of the two assumptions. First of all, we assumed that R_{series} is bias voltage independent, which might not be true. Second, we assumed that we know the potential barrier profile. Despite this model's weaknesses, a comparison with a much more difficult calculation and more direct measurements gives unexpectedly convergent results. Thus, our fittings for a few MWIR $InAs_{10ML}/GaSb_{10ML}$ samples (with essentially different R_{shunt} and R_{series} values) gave an average $m_{red} \approx 0.0148m_0$, nearly independent of temperature (it is the subject of a different contribution).

The electron effective masses of the MWIR $InAs_{x\_ML}/GaSb_{x\_ML}$ T2SLs (or very similar) for the in-plane direction ($m^*_{c1//}$) were measured by several authors. Suchalkin *et al.*[22] reported $m^*_{c1//}$ equal from about $0.025m_0$ to $0.028m_0$ depending on the sample, Omaggio *et al.*[23] estimated it from about $0.027m_0$ to $0.033m_0$, and Fuchs *et al.*,[24] based on magneto-optics measurements and 8 × 8 *Kp* calculation, obtained 0.0235 m_0. Additionally, they estimated $m^*_{hh1//}$ as about $0.0342m_0$. Putting average values into eq. (7), one can see that m^*_{red} should be on the order of $0.015m_0$, which agrees very well with our results.

6. Conclusions

In this work, we analyzed the dark current of MWIR type-II InAs/GaSb SL pin photodiodes in the temperature range from 120 to 240 K and bias voltage from –1.6 to +0.3 V. Our calculations were mainly focused on obtaining the reduced mass value from current-voltage characteristics for the C1-HH1 transition in $InAs_{10ML}/GaSb_{10ML}$ samples. We showed that simplified formalism, based on a bulk material model, is sufficient for estimating such reduced mass, but an essential step in this procedure is connected with taking into account the anisotropy of the band structure and the series resistance. Our fittings gave $m_{red} \approx 0.0148m_0$, which agree well with much more complex simulations and cyclotron resonance measurements.

Acknowledgements

This study was carried out with financial support from the National Science Center (grant DEC-2012/05/N/ST7/01057) and the Polish Ministry of Sciences and Higher Education Key Project POIG.01.03.01-14-016/08, ''New Photonic Materials and their Advanced Applications''.

References

1 G. A. Saihalasz, R. Tsu and L. Esaki: Appl. Phys. Lett. **30** (1977) 651.
2 L. L. Chang, N. Kawai, G. A. Saihalasz, R. Ludeke and L. Esaki: Appl. Phys. Lett. **35** (1979) 939.
3 A. Rogalski and P. Martyniuk: Infrared Phys. Technol. **48** (2006) 39.

4 A. Rogalski: Infrared Detectors (CRC Press, Boca Raton, 2009) 2nd ed., p. 808.
5 P. Martyniuk and A. Rogalski: Opto-Electron Rev. **21** (2013) 239.
6 F. Szmulowicz, H. J. Haugan, S. Elhamri and G. J. Brown: Phys. Rev. B **84** (2011) 14.
7 C. L. Canedy, E. H. Aifer, J. H. Warner, I. Vurgaftman, E. M. Jackson, J. G. Tischler, S. P. Powell, K. Olver, J. R. Meyer and W. E. Tennant: Infrared Phys. Technol. **52** (2009) 326.
8 A. Hood, D. Hoffman, B. M. Nguyen, P. Y. Delaunay, E. Michel and M. Razeghi: Appl. Phys. Lett. **89** (2006) 233513.
9 J. Nguyen, D. Z. Ting, C. J. Hill, A. Soibel, S. A. Keo and S. D. Gunapala: Infrared Phys. Technol. **52** (2009) 317.
10 D. R. Rhiger, R. E. Kvaas, S. F. Harris and C. J. Hill: Infrared Phys. Technol. **52** (2009) 304.
11 C. Cervera, K. Jaworowicz, H. Ait-Kaci, R. Chaghi, J. B. Rodriguez, I. Ribet-Mohamed and P. Christol: Infrared Phys. Technol. **54** (2011) 258.
12 B. Klein, E. Plis, M. N. Kutty, N. Gautam, A. Albrecht, S. Myers and S. Krishna: J. Phys. D. Appl. Phys. **44** (2011) 5.
13 M. Motyka, G. Sek, J. Misiewicz, A. Bauer, M. Dallner, S. Hofling and A. Forchel: Appl. Phys. Express **2** (2009) 126505.
14 Q. Yang, C. Pfahler, J. Schmitz, W. Pletschen and F. Fuchs: Proc. SPIE **4999** (2003) 448.
15 H. J. Hovel, R. K. Willardson and A. C. Beer: Semicond. Semimet. **11** (1975) 254.
16 B.-M. Nguyen: Ph.D. Thesis, Northwestern University, Evanston, Illinois, USA (2010).
17 T. V. C. Rao, S. V. Nair, H. E. Ruda, J. Antoszewski, J. B. Rodriguez, E. Plis, S. Krishna and L. Faraone: Semicond. Sci. Technol. **27** (2012) 7.
18 J. Wrobel, P. Martyniuk, E. Plis, P. Madejczyk, W. Gawron, S. Krishna and A. Rogalski: Proc. SPIE 8353 (2012) 835316.
19 M. A. Kinch: Semicond. Semimet. **18** (1981) 313.
20 Q. K. Yang, F. Fuchs, J. Schmitz and W. Pletschen: Appl. Phys. Lett. **81** (2002) 4757.
21 J. Wróbel, P. Martyniuk and A. Rogalski: Adv. Opt. Technol. **2012** (2012) 5.
22 S. Suchalkin, G. Belenky, S. P. Svensson, B. Laikhtman, D. Smirnov, L. C. Tung and S. Bandara: J Appl. Phys. **110** (2011) 043720.
23 J. P. Omaggio, R. J. Wagner, J. R. Meyer, C. A. Hoffman, M. J. Yang, D. H. Chow and R. H. Miles: Semicond. Sci. Technol. **8** (1993) S112.
24 F. Fuchs, E. Ahlswede, U. Weimar, W. Pletschen, J. Schmitz, M. Hartung, B. Jager and F. Szmulowicz: Appl. Phys. Lett. **73** (1998) 3760.